Journal of Molecular Liquids 360 (2022) 119454

Contents lists available at ScienceDirect

Journal of Molecular Liquids

journal homepage: www.elsevier.com/locate/molliq

# α-Amylase inhibition, anti-glycation property and characterization of the binding interaction of citric acid with α-amylase using multiple spectroscopic, kinetics and molecular docking approaches

Oghenetega J. Avwioroko [a,h,*], Akpovwehwee A. Anigboro [b], Chiagoziem A. Otuechere [a,h], Francis O. Atanu [c], Oluropo F. Dairo [d], Temidayo T. Oyetunde [e,h], Omotayo B. Ilesanmi [f], Augustine Apiamu [b], Akpoyovware S. Ejoh [g], Damilare Olorunnisola [e,h], Moses O. Alfred [e,h], Martins O. Omorogie [e,h], Nyerhovwo J. Tonukari [b]

[a] Department of Biochemistry, Faculty of Basic Medical Sciences, Redeemer's University, Ede, Osun State, Nigeria
[b] Department of Biochemistry, Faculty of Science, Delta State University, P.M.B.001, Abraka, Nigeria
[c] Department of Biochemistry, Faculty of Natural Sciences, Kogi State University, P.M.B. 1008, Anyigba, Nigeria
[d] Department of Physical Sciences, Faculty of Natural Sciences, Redeemer's University, Ede, Osun State, Nigeria
[e] Department of Chemical Sciences, Faculty of Natural Sciences, Redeemer's University, Ede, Osun State, Nigeria
[f] Department of Biochemistry, Faculty of Sciences, Federal University Otuoke, Bayelsa State, Nigeria
[g] Department of Biological Sciences, Covenant University, Ota, Ogun State, Nigeria
[h] Center for Chemical and Biochemical Research (CCBR), Redeemer's University, Ede, Osun State, Nigeria

ARTICLE INFO

*Article history:*
Received 3 December 2021
Revised 6 May 2022
Accepted 21 May 2022
Available online 27 May 2022

*Keywords:*
α-Amylase inhibition
Citric acid
Anti-glycation
Hyperglycemia
Spectroscopy
Molecular docking

ABSTRACT

The quest to suppress complications associated with diabetes mellitus is ever increasing, while food additives and preservatives are currently being considered to play additional roles besides their uses in food enhancement and preservation. In the present study, the protective prowess of a common food preservative (citric acid, CA) against advanced glycation end-products (AGEs) formation and its binding interaction mechanism with α-amylase (AMY), an enzyme linked with hyperglycemia management, were examined. Enzyme inhibition kinetics, intrinsic fluorescence, synchronous and 3D fluorescence spectroscopies, ultraviolet–visible (UV–Vis) absorption spectroscopy, Fourier transform-infrared (FT-IR) spectroscopy, thermodynamics, and molecular docking analyses were employed. Results obtained showed that citric acid decreased α-amylase activity via mixed inhibition ($IC_{50}$ = 5.01 ± 0.87 mM, $K_{ic}$ = 2.42 mM, $K_{iu}$ = 160.34 mM) and suppressed AGEs formation ($IC_{50}$ = 0.795 ± 0.001 mM). The intrinsic fluorescence of free α-amylase was quenched via static mechanism with high bimolecular quenching constant ($K_q$) and binding constant ($K_a$) values. Analysis of thermodynamic properties revealed that AMY-CA complex was spontaneously formed (ΔG < 0), entropy driven (TΔS > ΔH), with involvement of electrostatic forces. UV–Vis, FT-IR and 3D fluorescence spectroscopies affirmed alterations in α-amylase native conformation due to CA binding interaction. CA interacted with His-101, Asp-197, His-299, and Glu-233 within AMY active site. Our findings indicated that CA could impair formation of AGEs and interact with α-amylase to slow down starch hydrolysis; vital properties in management of type 2 diabetes complications.



## 1. Introduction

Diabetes mellitus (DM) is a metabolic disorder characterized by elevated blood glucose level and has been reported to be associated with other health complications such as delay in wound healing, diabetic retinopathy, development of diabetic cataract, and undesirable glycation of functional proteins, amongst others, after a prolong duration [1-4]. Over the years, the use of some therapeutic agents or nutraceuticals that are capable of inhibiting the activity of carbohydrate-metabolizing enzymes (such as α-amylase, α-glucosidase, aldose reductase etc) has helped in preventing post-prandial hyperglycemia in diabetics [5-7]. α-Amylase (AMY) is a hydrolase that breaks down polysaccharide via cleavage of their

* Corresponding author at: Department of Biochemistry, Faculty of Basic Medical Sciences, Redeemer's University, Ede, Osun State, Nigeria.
*E-mail addresses:* avwiorokoo@run.edu.ng, joavwioroko@gmail.com (O.J. Avwioroko).

https://doi.org/10.1016/j.molliq.2022.119454
0167-7322/

α-1,4-glycosidic bonds to release simple sugars and disaccharides [4,8]. Inhibition of the enzymatic activity of α-amylase in diabetic patients therefore helps in slowing down the after-meal digestion of polysaccharides to simple sugar, thereby preventing the sudden rise in blood glucose level that poses threat to survival [9,10]. While drugs like acarbose had been successfully used in this regard, its side effects, such as flatulence and abdominal discomfort, are probably due to its excessive inhibitory effect on the enzyme (α-amylase) [4,11]. Hence, further researches are necessary to discover other substances or compounds (including synthetic food additives) that may be able to inhibit the activity of the carbohydrate-degrading enzyme moderately but not excessively. A previous study had reported that citric acid (CA) could inhibit alpha-amylase activity [12]. However, to the best of our knowledge, the inhibition kinetics, mode of inhibition, binding constant, thermodynamics, fluorescence quenching mechanism, anti-glycation properties, and binding interaction of citric acid with active site domain amino acid residues of α-amylase are yet to be documented.

Hence, in the present study, we elucidated the binding characteristics of citric acid, a common food preservative, with α-amylase enzyme using multiple spectroscopic techniques including intrinsic fluorescence spectroscopy, synchronous fluorescence spectroscopy, three-dimensional (3D) fluorescence spectroscopy, ultraviolet–visible light (UV–Vis) absorption spectroscopy, and Fourier-Transform infrared (FT-IR) spectroscopy. Enzyme inhibition kinetics and mode of inhibition were evaluated by following the Michaelis-Menten (M–M) model of kinetics. Protein-ligand binding association constant, driving forces involved, number of binding sites involved, binding affinity and participating active site amino acid residues were delineated using a combination of spectroscopic, thermodynamics and molecular docking approaches. The inhibitory potential of citric acid against fructose-induced advanced glycation end-products (AGEs) formation *in vitro* was also evaluated. The study discussed in detail, the binding interaction of citric acid with amino acid residues present at α-amylase active site domain as well as its implication in regulation of polysaccharide hydrolysis and postprandial hyperglycemia.

## 2. Materials and methods

### 2.1. Material and reagents used

α-Amylase (lyophilized powder form) from *Bacillus subtilis* (TIMSTAR Laboratories, Winsford, UK) was used in this study. Citric acid and buffer salts were obtained from Central Drug House (CDH) (P) Ltd., New Delhi, India. 3,5-Dinitrosalycylic acid (P774, 99% HPLC grade) used was from AK Scientific (California, USA). All other reagents used were of analytical grades.

### 2.2. Protein binding and interaction studies

#### 2.2.1. Intrinsic fluorescence spectroscopy

Intrinsic fluorescence spectra were measured in the present study following the procedure of Shi et al. [13] and Makarska-Bialokoz *et al.* [14] with minor modifications. α-Amylase (AMY) ($8.93 \times 10^{-6}$ M, freshly prepared with 0.2 M phosphate buffer, pH 7.4) was titrated with varying concentrations of citric acid (CA) and thereafter incubated for 30 min. The final active concentrations of CA in the reaction mixtures were $189.30 \times 10^{-6}$, $473.20 \times 10^{-6}$, $757.10 \times 10^{-6}$, $1041.00 \times 10^{-6}$, $1200.00 \times 10^{-6}$ and $1600.00 \times 10^{-6}$ M designated as CA1, CA2, CA3, CA4, CA5 and CA6, respectively. The emission fluorescence intensity readings were carried out with the aid of a Cary Eclipse Fluorescence Spectrophotometer (Agilent Technologies) at an excitation wavelength of 280 nm and emission wavelength range of 300 to 450 nm. The investigation was carried out at three different temperatures (298, 303 and 310 K) and thereafter the spectral readings were analyzed for protein–ligand binding interaction parameters and thermodynamic parameters using Stern-Volmer, modified Stern-Volmer and Van't Hoff equations. Spectral readings of free α-amylase (AMY) in the absence of CA (with phosphate buffer replacing CA) at the same experimental conditions served as control.

#### 2.2.2. 3D fluorescence spectroscopy

The three-dimensional (3D) fluorescence spectra of samples were measured based on the method of Makarska-Bialokoz *et al.* [14] with slight modifications. Briefly, α-amylase ($8.93 \times 10^{-6}$ M, pH 7.4) was reacted with $473.20 \times 10^{-6}$ M citric acid at 298 K for 30 min duration. Thereafter, the 3D fluorescence spectra of AMY in the presence and absence of CA were read using the Cary Eclipse Fluorescence Spectrophotometer (Agilent Technologies) at an excitation wavelength range of 200–600 nm over an emission wavelength of 200 – 600 nm with increments of 5 nm. The slit widths used for both excitation and emission were 5 nm / 5 nm, respectively.

#### 2.2.3. Inner filter effects

It was necessary that the inner filter effects be removed from the fluorescence data, hence the fluorescence data were corrected for the inner filter effects using the equation [13,15,16]:

$$F_{cor} = F_{obs} \times 10^{(A_{ex}+A_{em})/2} \quad (1)$$

where, $F_{obs}$ and $F_{cor}$ represent the respective observed and corrected fluorescence intensities, while $A_{ex}$ and $A_{em}$ denote the excitation and emission wavelengths of the system, respectively.

#### 2.2.4. Ultraviolet–visible absorption spectroscopy

The UV–vis absorption spectra measurements were carried out following the method of Shi *et al.* [13] and Wang *et al.* [17] with slight modifications. Briefly, the UV–vis absorption spectra measurements of α-amylase ($8.93 \times 10^{-6}$ M, pH 7.4) solutions in the absence and presence of varying concentrations of citric acid were taken using a 3.0 mL quartz cuvette on a Shimadzu UV-1650pc spectrophotometer (Shimadzu, Kyoto, Japan). The concentration of the protein (AMY) was fixed, while CA was titrated at final concentrations of $189.30 \times 10^{-6}$, $473.20 \times 10^{-6}$, $757.10 \times 10^{-6}$, $1041.00 \times 10^{-6}$, $1200.00 \times 10^{-6}$ and $1600.00 \times 10^{-6}$ M designated as CA1, CA2, CA3, CA4, CA5 and CA6, respectively. The UV spectra were recorded from 190 to 400 nm at room temperature (298 K).

#### 2.2.5. FT-IR spectroscopy

Fourier Transform-infrared spectra measurements carried out in the present study using Shimadzu FTIR-8400S model FT-IR spectrometer. α-Amylase ($8.93 \times 10^{-6}$ M, pH 7.4) was titrated with varying concentrations of citric acid at room temperature. The final active concentrations of CA in the reaction mixtures were $189.30 \times 10^{-6}$ and $473.20 \times 10^{-6}$ M denoted as CA1 and CA2, respectively. Thereafter, the FT-IR spectra of α-amylase in the absence and presence of CA were read between 4500 and 400 $cm^{-1}$ with a resolution of 1 $cm^{-1}$. All the spectral measurements were performed at 298 K. Multiple peaks within amide I band region of the FT-IR spectra were deconvoluted and analyzed using Gaussian peak function with the aid of OriginPro 9.1 software.

#### 2.2.6. Synchronous fluorescence spectroscopy

Measurements of synchronous fluorescence spectra were used to analyze the respective microenvironments of tyrosine and tryp-

tophan residues of α-amylase in the presence of the ligand, as described by Huang et al [18]. The excitation and emission wavelength intervals (Δλ) were set at 15 and 60 nm. Thereafter, synchronous fluorescence intensity was read over an emission wavelength range of 220 – 340 nm. The ratio of synchronous florescence quenching (RSFQ) was calculated using the following equation [2,19]:

$$\text{RSFQ} = 1 - \left(\frac{F}{F_o}\right) \tag{2}$$

where F0 and F denote the synchronous fluorescence intensities of α-amylase in the absence and presence of citric acid, respectively.

### 2.3. Anti-glycation and α-amylase inhibition studies

#### 2.3.1. In vitro anti-glycation assay of CA

The anti-glycation activity of citric acid was determined using the bovine serum albumin (BSA)-fructose induced glycation model previously described by Zeng *et al.* [20], with minor modifications. BSA (20 mg $mL^{-1}$) and fructose (0.5 M) were incubated in 0.2 M potassium phosphate buffer (pH 7.4) at 323 K for 24 h in the absence or presence of varying final concentrations of citric acid (189.30, 473.20, 757.10, 800.00 and 900.00 μM). After the period of incubation, the fluorescence intensities of the reaction mixtures were measured over an emission wavelength range of 370–650 nm at an excitation wavelength of 360 nm. The fluorescence intensity corresponded to the amount of fluorescent advanced glycation end-products (AGEs) formed. Aminoguanidine hydrochloride (AG), a standard anti-glycation agent, was used as a positive control at final concentrations of 1, 2, 3, 4 and 5 mM. Inhibition of AGEs formation was calculated as follows:

$$\text{Relative antiglycation activity}\,(\%) = \frac{F_c - F_s}{F_c} \times 100\% \tag{3}$$

where $F_c$ and $F_s$ denote the fluorescence intensity of control and fluorescence intensity of the test sample (CA) or standard (AG), respectively, at an emission wavelength of 453 nm.

#### 2.3.2. Assay for α-amylase inhibition by CA

The inhibitory effect of citric acid on α-amylase was done following the method of Adefegha and Oboh [6] and Oboh *et al.* [11] with minor modification. Briefly, 500 μL of α-amylase [8.93 μM, prepared with 20 mM phosphate buffer (pH 7.4) containing 0.006 M sodium chloride) was mixed with equal volume of varying final concentrations of citric acid (2.08, 3.12, 4.16, 4.70, 5.21 and 5.50 mM) and thereafter incubated at 310 K for 10 min. Later, slightly pre-heated and cold soluble starch solution (500 μL, 1%) was added to the reaction mixture, shaken to mix and re-incubated for additional 10 min at 310 K. The hydrolytic reaction was terminated by adding 200 μL of dinitrosalicylic acid (DNS) reagent [3,5-dinitrosalicylic acid (1%) and sodium potassium tartrate (12%) dissolved with 0.4 M NaOH] [21]. The reaction mixtures were then incubated for 5 min in a hot water bath at 368–371 K to develop the colour and absorbance readings were taken at 540 nm (against water blank) after adding 3 mL of distilled water to the reaction test tubes. The percentage inhibition of enzyme activity was calculated as follows:

$$\propto -\textit{Amylase inhibition}(\%) = \left(\frac{A_{control} - A_{sample}}{A_{control}}\right) \times 100\% \tag{4}$$

where $A_{sample}$ and $A_{control}$ denote the absorbance values of the test samples and blank (reaction mix without sample) read after cooling the reaction tubes down to ambient temperature. All the tests were carried out in three replicates.

#### 2.3.3. Analysis of α-amylase mode of inhibition by CA and inhibition constants

The assay for the determination of the mode of inhibition of α-amylase by citric acid was carried out following previously described methods for enzyme inhibition kinetics [7,22] with little modification. Briefly, α-amylase activity was determined as described in Section 2.3.2 using varying concentrations of the substrate (soluble starch; 0.60, 0.80, 1.00, 1.20 and 1.40%) in the presence of different concentrations of citric acid (0.00, 3.12, 4.16, 4.70 and 5.50 mM). One unit of α-amylase activity was expressed as the rate at which 1 mmole of glucose was released from starch per minute per litre. Data from the kinetics assay were analyzed using the respective derivatives of Michaelis-Menten equation for enzyme kinetics (Eq. (5)) and enzyme mixed inhibition kinetics (Eq. (6)) as follows [22,23]:

$$\frac{1}{V} = \frac{1}{V_{max}} + \frac{K_m}{V_{max}} \times \frac{1}{[S]} \tag{5}$$

$$V = \frac{V_{max}[S]}{K_m\left(1 + \frac{1}{K_{ic}}\right) + [S]\left(1 + \frac{1}{K_{iu}}\right)} \tag{6}$$

where V, $V_{max}$ and $K_m$ represent the initial enzyme activity, maximum enzyme activity and Michaelis-Menten constant, respectively. Values of the inhibition constants for competitive and uncompetitive inhibitions ($K_{ic}$ and $_{Kic}$) were derived from secondary Lineweaver-Burk (LB) plots based on Eq. (7) and Eq. (8) as follow [22,23]:

$$\text{Gradient} = \left(1 + \frac{[I]}{K_{ic}}\right) \tag{7}$$

$$\textit{Vertical intercept} = \left(1 + \frac{[I]}{K_{iu}}\right) \tag{8}$$

Values of gradient and vertical intercept at each inhibitor concentration (used for the secondary LB plots) were, however, obtained from the primary Lineweaver-Burk plots based on Eq. (5).

### 2.4. Molecular docking analysis

Docking analysis was carried out using AutoDock4.2 module incorporated in the PyRx software. Three dimensional structures of citric acid and acarbose were downloaded from the PubChem database. Similarly, three dimensional structure of α-amylase (PDB ID: 1OSE) was downloaded from the RSCB Protein Data Bank (PDB). The energies of the ligands were minimized. The protein structure was prepared for docking by removing water molecules, crystallized ligands and other co-crystallized molecules before the carrying out the docking experiments. Docking simulations was carried out in a computation grid box at the active site of the enzyme with x, y and z dimensions of 33.13, 36.0 and 28.50, respectively. The x, y and z center dimensions were 35.29, 38.98 and 4.66; docking was performed at exhaustiveness of 8. Structures of the docked ligands were visualized using PyMol and Discovery studio 5.0.

### 2.5. Statistical analysis

Values of experimental data were expressed as mean ± standard deviation of mean for triplicate analyses (n = 3). All spectra plots were made using OriginPro. 9.1 version, while enzyme kinetics plots were made using Microsoft Excel. Slopes, intercepts and their standard error values were computed using LINEST in Microsoft Excel.

## 3. Results and discussion

### 3.1. Probing the binding interaction between AMY and CA by fluorescence spectroscopy

#### 3.1.1. Fluorescence quenching mechanism and quenching constants

Fluorescence spectroscopy is one of the major and highly reliable spectroscopic techniques used in investigating the molecular interactions between a macromolecule (such as proteins) and a ligand (small molecule) [24-27]. The technique provides important information about the structure of polypeptides by detecting variations in emission fluorescence peaks. When the fluorescence intensity of a fluorophore (the macromolecule) decreases due to its interaction with a quencher (a ligand), the process is referred to as fluorescence quenching [1,15,24,28]. Most α-amylases (including human pancreatic α-amylase) are composed of over 300 amino acid residues with aspartate, asparagine, glutamate, tyrosine, histidine, arginine, phenylalanine, serine and tryptophan predominantly found at or near the active site domain of the enzyme [29]. Specifically, Asp197, Glu233 and Asp300 make up the catalytic triad used for hydrolysis by α-amylases [29]. While Asp197 residue acts as a nucleophile in catalysis, Glu233 and Asp300 play the role of an acid/base catalyst [29]. The inherent fluorescing property of proteins including enzymes such as α-amylase is mainly due to their rich-content of aromatic amino acid residues such as tyrosine (Tyr), tryptophan (Trp) and phenylalanine (Phe). When excited at a wavelength of 280 nm in the presence of increasing concentrations of a quencher, information about the tryptophan and tyrosine residues of α-amylases can be obtained by recording the fluorescence emission peaks at 340 nm [24,25,30] and changes in the fluorescence properties of the protein can be attributed to the binding of the small molecule (ligand) to the protein. In the present study, we investigated the binding interaction of citric acid (a commonly used food preservative or additive) to α-amylase. As shown in Fig. 1, the intrinsic fluorescence spectrum of α-amylase was quenched as the intensity decreased from 100% to 63.76, 68.82 and 61.61% respectively in the presence of 1041 μM citric acid (CA4) at all three temperatures investigated (298, 303 and 310 K). Likewise, CA at other concentrations examined (such as CA5 and CA6) also quenched the intensity of AMY fluorescence via a similar trend but in a concentration-dependent manner. Fig. 1 revealed that 1600 μM citric acid (CA6) reduced AMY fluorescence intensity from 100% to 56.79, 63.26 and 66.37% at 298, 303 and 310 K, respectively. The observed reduction in fluorescence intensity is clearly due to the binding of citric acid to α-amylase which resulted in alteration of the protein's microenvironment. Three types of fluorescence quenching mechanisms had been described by which fluorescence quenching occurs; namely, static quenching, dynamic quenching or mixed quenching [24,25,27,31-35]. Static and dynamic mechanisms can be distinguished either by the temperature-dependent variation in Stern-Volmer's quenching constant ($K_{sv}$) values or the value(s) of the bimolecular quenching constant ($K_q$) at a given temperature or both as depicted by the Stern-Volmer's equation (Eq. (9)) as follows [13,17,36]:

$$\frac{F_0}{F} = 1 + K_{SV}[Q] = 1 + K_q\tau^0[Q] \tag{9}$$

where $F_0$, and F represent the emission fluorescence intensity of the fluorophore or macromolecule (AMY) in the absence and presence of the quencher (CA), respectively; [Q] is the concentration of the quencher (citric acid) and $\tau^0$ represents the lifetime of the fluorophore in the absence of the quencher ($\tau^0 = 10^{-8}$ s for a biomolecule) [13,36]. As shown in Fig. 2, the Stern-Volmer plots (Fig. 2A) at different temperatures (obtained based on Eq. (9)) for the quenching of AMY by CA indicated a linear relationship ($R^2$ = 0.9892 to 0.9954) with increasing concentrations of CA, suggesting that the binding interaction took place via a single quenching mechanism (either static or dynamic) [13,14,30]. The obtained values of the bimolecular quenching constant ($K_q$) of AMY in the presence of CA were (5.06 ± 0.21) × $10^{10}$, (4.24 ± 0.13) × $10^{10}$, and (3.37 ± 0.15) × $10^{10}$ $M^{-1}$ $Sec^{-1}$ at 298, 303 and 310 K, respectively (Table 1). The $K_q$ values are 1.69 – 2.53 times higher than the maximum dynamic quenching rate constant of 2.0 × $10^{10}$ $M^{-1}$ $Sec^{-1}$, suggesting that CA effectively quenched the emission fluorescence of AMY due to formation of AMY-CA complex [14,24]. Furthermore, the $K_{sv}$ values slightly decreased as temperature increased from 298 to 310 K (Table 1). This observation is characteristic of static quenching mechanism which involves formation of complex between the fluorophore and quencher, unlike in dynamic quenching where $K_{sv}$ values are directly proportional to temperature increment [14,19,24]. In fluorescence quenching experiments where mixed quenching (a combination of both static and dynamic quenching mechanisms) is involved, $K_{sv}$ values may increase as temperature increases yet $K_q$ values are<2.0 × $10^{10}$ $M^{-1}$ $Sec^{-1}$, or $K_{sv}$ values would decrease as temperature increases yet $K_q$ values are>2.0 × $10^{10}$ $M^{-1}$ $Sec^{-1}$ [13,32-35,37]. The results obtained in the present study, however, indicated that the intrinsic fluorescence of α-amylase was mainly quenched via static mechanism by citric acid. The findings of the study are in agreement with those of Lu et al. [38] who reported a similar quenching mechanism for α-amylase fluorescence intensity in the presence of gallic acid. The $K_q$ value of gallic acid for α-amylase was, however, higher than that of citric acid for the same enzyme at physiological pH although both values were higher than the maximum scatter collision quenching constant in water (2.0 × $10^{10}$ $M^{-1}$ $Sec^{-1}$) for a dynamic mechanism [38].

#### 3.1.2. Number of binding site and interaction constant

The binding constant ($K_a$) and number of binding sites (n) for the interaction between AMY and CA were determined following the method described earlier by Bi et. al. [39] and Feroz et al. [40] which eliminates the limitations (or inaccuracy) associated with the modified Stern-Volmer equation regarding Ka and n estimations [14,15,25,41]. The method involves the use of the following double–logarithm regression plot equations as shown in Eq. (10) and Eq. (11) [39,40]:

$$Log\frac{F_0 - F}{F} = nLogK_a - nLog[Q_f] \tag{10}$$

$$[Q_f] = \left([Q_t] - \frac{(F_0 - F)[P_t]}{F_0}\right)^{-1} \tag{11}$$

Where $[Q_f]$ is the free concentration of the ligand (quencher), $[P_t]$ is the total concentration of the protein (fluorophore), while $F_0$ and F denote the respective emission fluorescence intensities of the macromolecule in the absence and presence of increasing total concentrations of the quencher $[Q_t]$.

In the present study, the regression plots of the interaction between AMY and CA based on Eq. (10) and Eq. (11) at the three temperatures investigated were made (Fig. 2B) and the binding constant ($K_a$) and number of binding site (n) were deduced from the values of intercept (nLog $K_a$) and slope (-n) respectively (Table 1). The value of n at all temperatures investigated (298, 303 and 310 K) was within the range of 0.68 – 0.84, which is approximately equal to one. This showed that one molecule of the citric acid interacted with AMY via a single binding site. Also, the values of the binding constant ($K_a$) between citric acid and AMY (Table 1) were slightly high and temperature dependent; indicating the degree of stability of the complex formed [14]. However, when compared with gallic acid as reported by Lu et al. [38],

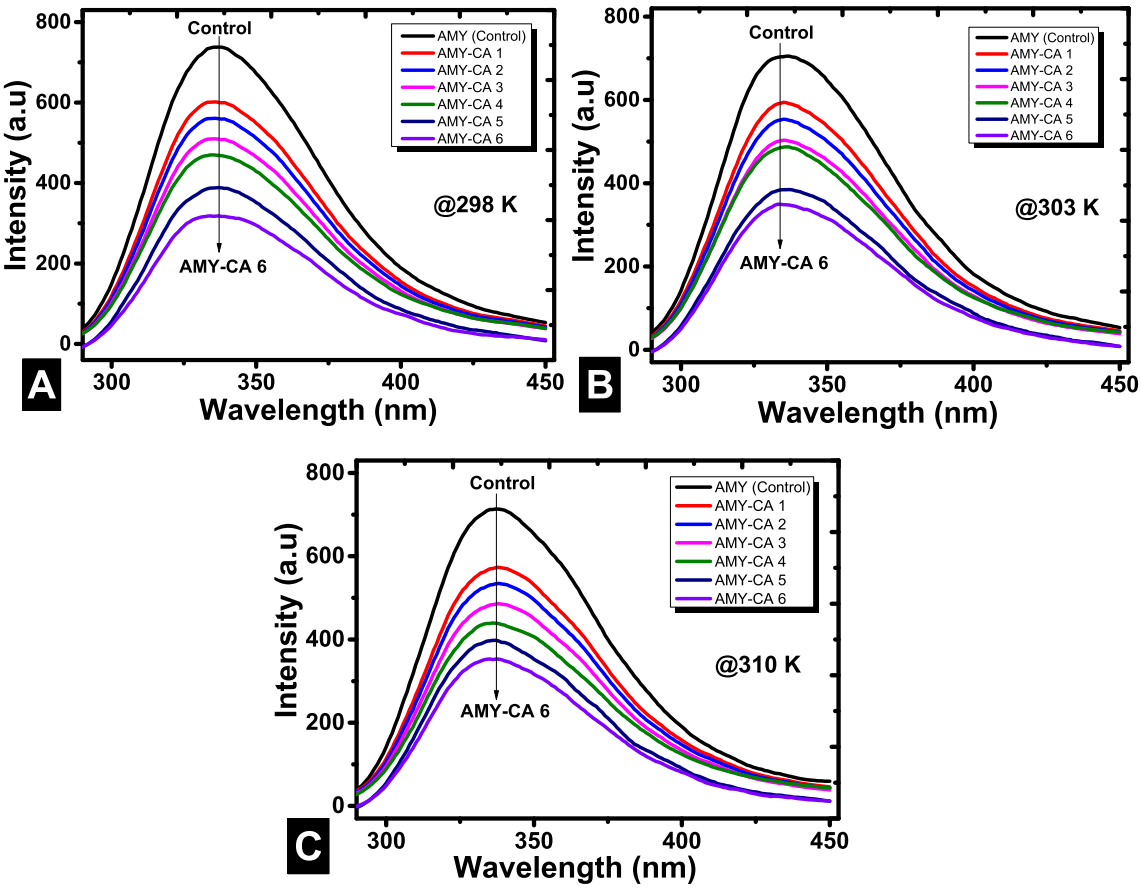


**Fig. 1.** Intrinsic fluorescence intensity of α-amylase in the absence and presence of citric acid (CA) at three different temperatures (298, 303 and 310 K).

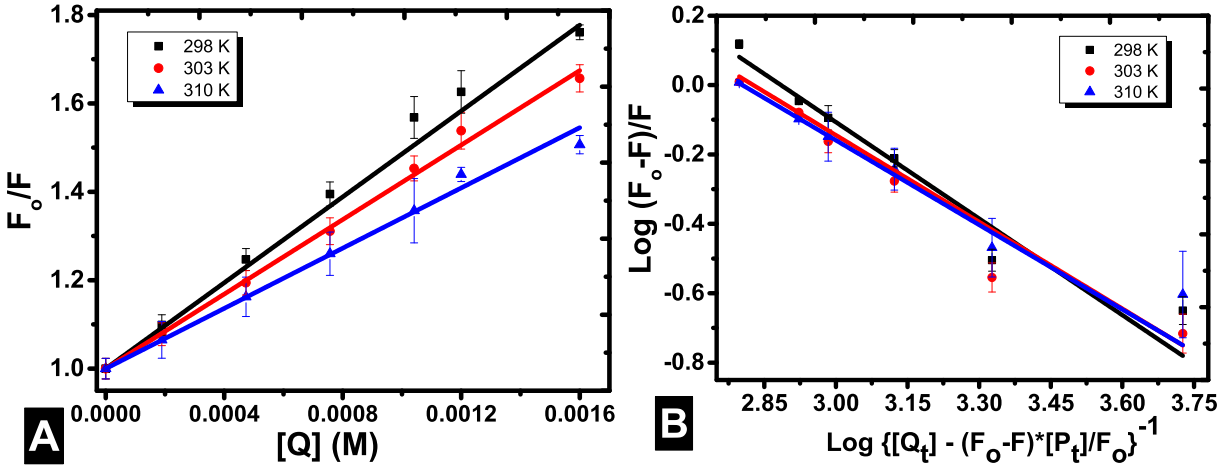


**Fig. 2.** Stern-Volmer (A) and modified Stern-Volmer (B) plots for the quenching of alpha-amylase by citric acid at three different temperatures, $\lambda_{ex}$ = 280 nm, $\lambda_{em}$ = 300–450 nm, and pH 7.4.

**Table 1**
Stern-Volmer quenching constant ($K_{sv}$), bimolecular quenching constant ($K_q$), number of binding sites (n), and binding constant ($K_a$) for the interaction between α-amylase and citric acid at different temperatures.

| Temp. (K) | $K_{sv}$ ($M^{-1}$) | $K_q$ ($M^{-1}$ $Sec^{-1}$) × $10^{10}$ | $R_a^2$ | n | $K_a$ ($M^{-1}$) | $R_b^2$ |
|---|---|---|---|---|---|---|
| 298 | 506.21 ± 20.67 | 5.06 ± 0.21 | 0.9903 | 0.84 ± 0.10 | 744.22 ± 0.32 | 0.9434 |
| 303 | 424.30 ± 12.85 | 4.24 ± 0.13 | 0.9954 | 0.82 ± 0.09 | 611.10 ± 0.27 | 0.9583 |
| 310 | 337.29 ± 15.10 | 3.37 ± 0.15 | 0.9892 | 0.68 ± 0.07 | 582.07 ± 0.22 | 0.9597 |

the $K_a$ values of gallic acid acid for α-amylase binding are relatively higher than those of citric acid for α-amylase binding; this suggests that gallic acid-amylase complex would be slightly more stable than that of CA-AMY complex [38].

### 3.2. Influence of CA binding on AMY native conformation

#### 3.2.1. UV–vis absorption spectroscopy

Amongst several other multi-spectroscopic techniques, ultraviolet–visible absorption spectroscopy is a simple technique employed over the decades with high precision for evaluation and understanding of the molecular impact of a small molecule (ligand) binding on the secondary structure of macromolecules (proteins) [17,42]. Hence to gain insight into the molecular interaction between α-amylase and the commonly used food preservative (citric acid), we employed UV–vis absorption spectroscopy to measure the electronic transitions from the ground state of the protein (α-amylase) to its excited state [42]. The result in Fig. 3 showed that α-amylase had two absorption peaks at a physiological of pH 7.4 and room temperature. The first strong peak was obtained at a maximum absorption wavelength of about 207 nm which could be attributed to $\pi \rightarrow \pi^*$ transition of carbonyl group in the peptide backbone of AMY conformation, while the second maximum absorption peak obtained at about 278 nm was mainly due to the $\pi \rightarrow \pi^*$ transition of aromatic groups of amino acid residues (tryptophan, phenylalanine and tyrosine) in the protein [1,17]. The absorbance values (or absorption intensities) of the free enzyme (AMY) at wavelengths of 207 and 278 nm increased with increasing concentrations of the interacting citric acid (Fig. 3). This suggested that the native conformation of AMY was slightly altered in the presence of citric acid, hence indicating the high possibility of complex formation between the protein and CA as previously inferred from the fluorescence spectroscopy results.

#### 3.2.2. Fourier Transform-Infrared (FT-IR) spectroscopy

FT-IR spectroscopy is another valuable spectroscopic technique used in determining changes in the native conformation or secondary structure of macromolecules including proteins [25,43]. As shown in the Fourier Transform-Infrared (FT-IR) spectra of α-amylase (8.93 μM, pH 7.4, T = 298 K) in the absence and presence of citric acid (Fig. 4A), the binding interaction of citric acid to α-amylase at both concentrations investigated led to a shift in the broad peak at 3402 $cm^{-1}$ in the unbound enzyme (AMY) to a narrow peak at a wavenumber of 3454 $cm^{-1}$ in its bound states (AMY-CA1 and AMY-CA2) [Fig. 4A(A1)]. Peak positions between 3200 and 3550 $cm^{-1}$ were attributed to O–H stretching of hydroxyl groups in the enzyme molecule which consists of polar amino acid residues such as tyrosine, serine and threonine amongst other residues [42,43]. In proteins generally, two categories of amide bond peak positions exist. These are known as the amide I band or region characterized by absorption peaks between 1700 and 1600 $cm^{-1}$ (C = O stretching) and amide II band denoted by peaks between 1600 and 1500 $cm^{-1}$ (C–N stretching coupled with N–H bending mode) [25,43]. While both amide I and amide II bands are unique to all proteins, the amide I spectra region is more important and frequently reported in studies due to its high sensitivity to changes in protein secondary structure [42]. Hence during ligand–protein binding interactions, changes in peak positions within the amide I region are indicative of a compromised integrity of the protein's secondary structure or native conformation [2,25]. In the present study, the impact of the binding of citric acid on the amide I region of α-amylase is as shown in Fig. 4A (A2). The free enzyme had six peaks within the amide I band region of the FT-IR spectra at the following wavenumbers: 1659, 1654, 1632, 1624, 1619, and 1613 $cm^{-1}$. The peak positions and their numbers, however, changed to seven (1694, 1688, 1678, 1657, 1651, 1639, and 1632 $cm^{-1}$) in the AMY-CA1 complex and also in the AMY-CA2 complex (1688, 1673, 1657, 1649, 1640, 1638, and 1612 $cm^{-1}$) following interaction with citric acid. The observed alteration in the number of peaks and their positions in the amide I region of α-amylase suggests that the protein conformation was affected [7,25,43].

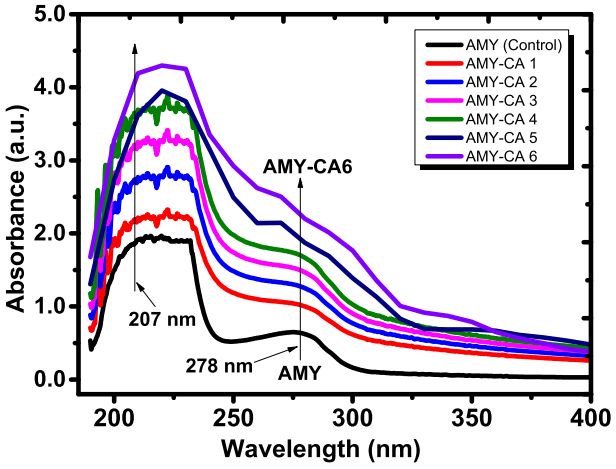


**Fig. 3.** UV–visible spectra of α-amylase ($8.93 \times 10^{-6}$ M, pH 7.4) in the absence and presence of citric acid.

Using Gaussian peak function, the FT-IR spectra which denoted the native α-amylase in the absence and presence of citric acid were deconvoluted in their amide I band region. This was to quantitatively estimate the conformational changes that occurred in the protein secondary structures due to the binding interactions [44,45]. Fig. 4B shows the deconvoluted FT-IR spectra of AMY, AMY-CA1 and AMY-CA2, respectively (Fig. 4B1-B3), while Table 2 gives a comparison of the secondary structure contents of α-amylase in the absence and presence of citric acid. Based on literature, bands at 1615–1637 $cm^{-1}$ are generally assigned to β-sheet, 1638–1648 $cm^{-1}$ to random coil, 1649–1660 $cm^{-1}$ to α-helix, 1660–1680 $cm^{-1}$ to β-turn, while bands at 1680–1692 $cm^{-1}$ are assigned to β-antiparallel, respectively [33,44,45]. Our result (Table 2) revealed an increase in α-helix and β-sheet contents, followed by a decrease in β-turn and random coil contents, of the secondary structures in AMY as it combines with increasing concentrations of citric acid (Table 2). The observed patterns of conformational changes in the secondary structures of α-amylase in the present study are in agreement with those observed in β-fold and random coil contents of bovine serum albumin upon its interaction with baricitinib, as reported by Zhang et al. [45]. This further suggests that the change in conformation of AMY arose from its binding with citric acid.

#### 3.2.3. Synchronous fluorescence spectroscopy

Synchronous fluorescence spectroscopy can be used protein–ligand binding studies to sensitively and uniquely monitor changes in the microenvironment of the protein (fluorophore) [18]. While synchronous fluorescence readings at $\Delta\lambda$ = 15 nm specifically provide information on changes in the microenvironment of tyrosine residues in protein molecules, characteristic changes in microenvironment of tryptophan residues are revealed at $\Delta\lambda$ = 60 nm [2,46]. As shown in Fig. 5, the maximum synchronous fluorescence intensity corresponding to tyrosine residues in AMY decreased from 269.65 to 71.45 in the presence of citric acid (CA6) at an emission wavelength of 292 nm. This was also accompanied by a red shift of 1 nm (from an emission wavelength of 292 nm in AMY to 291 nm in AMY-CA6) (Fig. 5A). The observed red shift indicates a decrease in the hydrophobicity (increase in polarity) within the microenvironment surrounding tyrosine residues in the enzyme, and an

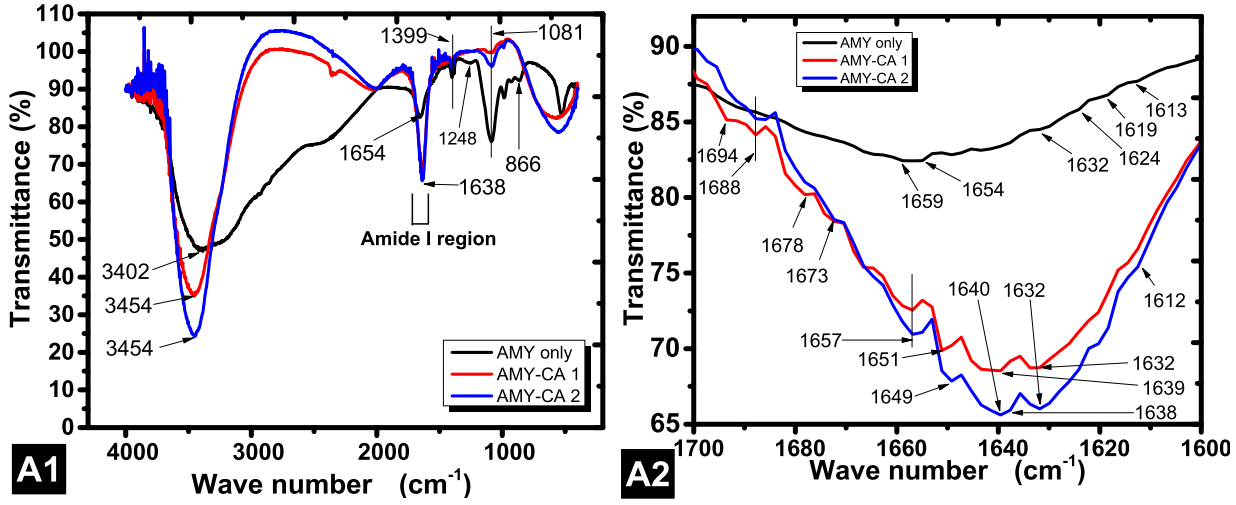


**Fig. 4A.** Fourier Transform-Infrared spectra of α-amylase ($8.93 \times 10^{-6}$ M, pH 7.4, T = 298 K) in the absence and presence of citric acid (CA). (A1) Impact of CA binding interaction on the whole protein molecule; (A2) impact of the binding interaction on amide I region (1700 – 1600 $cm^{-1}$) of α-amylase.

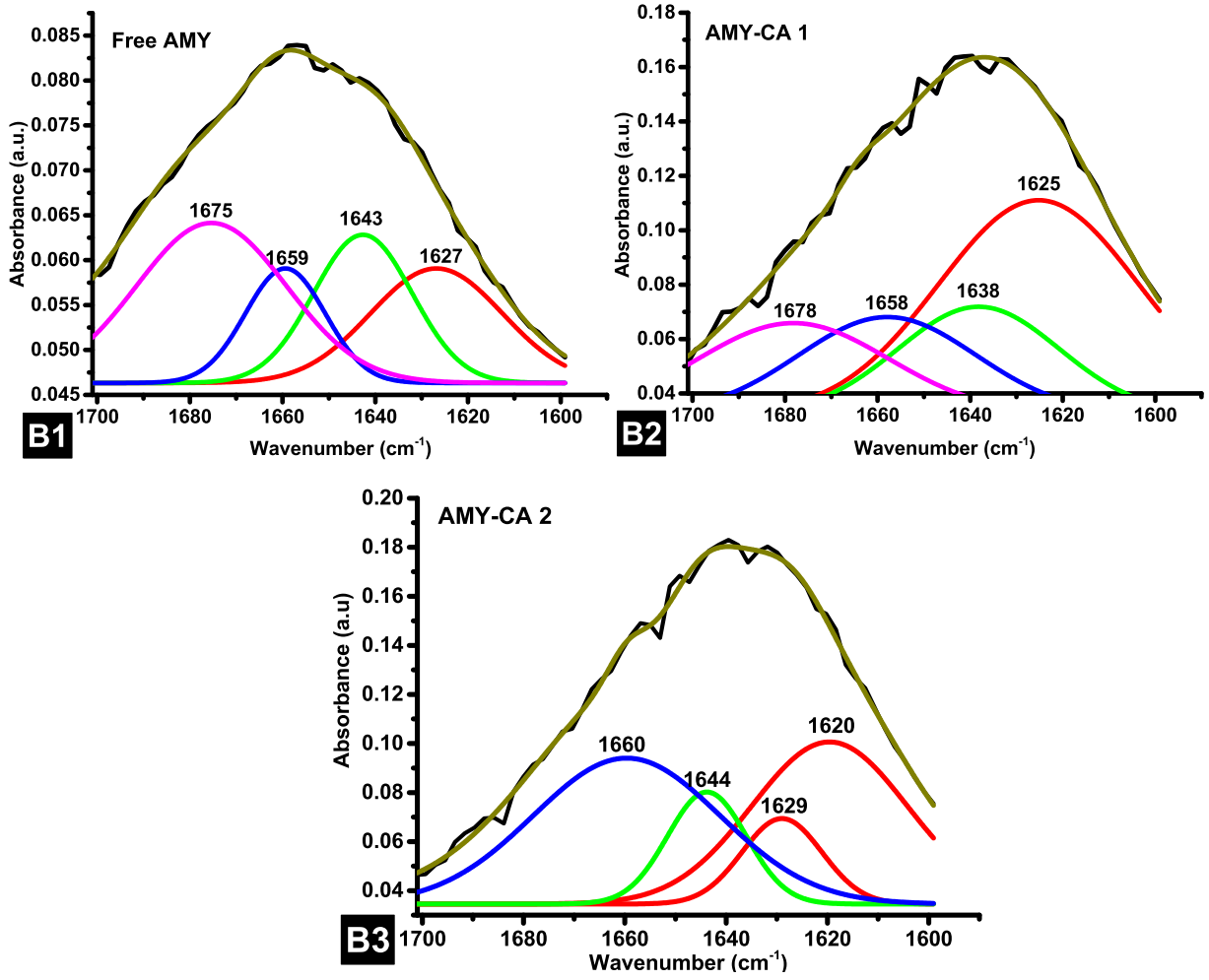


**Fig. 4B. Fitted FT-IR spectra of AMY (8.93 μM) in PBS (pH 7.4) in the absence (B1) and presence of citric acid [B2; 1:21 (AMY:CA1) and B3; 1:53 (AMY:CA2)] over a wavenumber range of 1701 to 1599 $cm^{-1}$.** Black lines represent the experimental results. Dark yellow lines are the fitting IR spectra. Other color lines such as magenta, blue, red and green represent the multiple peaks from IR spectra (black line) fitting using Gaussian peak function.

increase in the stretching extent of the peptide chain [13,47]. Similarly, the maximum synchronous fluorescence intensity corresponding to tryptophan residues in AMY also decreased from 677.74 in AMY to 370.94 in the presence of citric acid (AMY-CA6) at an emission wavelength of 273 nm (Fig. 5B). However, there was no observed shift in the intrinsic fluorescence spectra

**Table 2**
Changes in secondary structure components of α-amylase (8.93 μM) in the absence and presence of citric acid.

| AMY-CA complex | % α-Helix | % β-Sheet | % β-Turn | % Random coil |
|---|---|---|---|---|
| **Absence of CA** | | | | |
| 1:0 | 14.55 | 24.06 | 38.17 | 23.22 |
| **Presence of CA** | | | | |
| 1:21 | 18.18 | 45.25 | 18.29 | 18.28 |
| 1:53 | 40.02 | 47.01 | – | 12.97 |

AMY = α-Amylase; CA = citric acid.

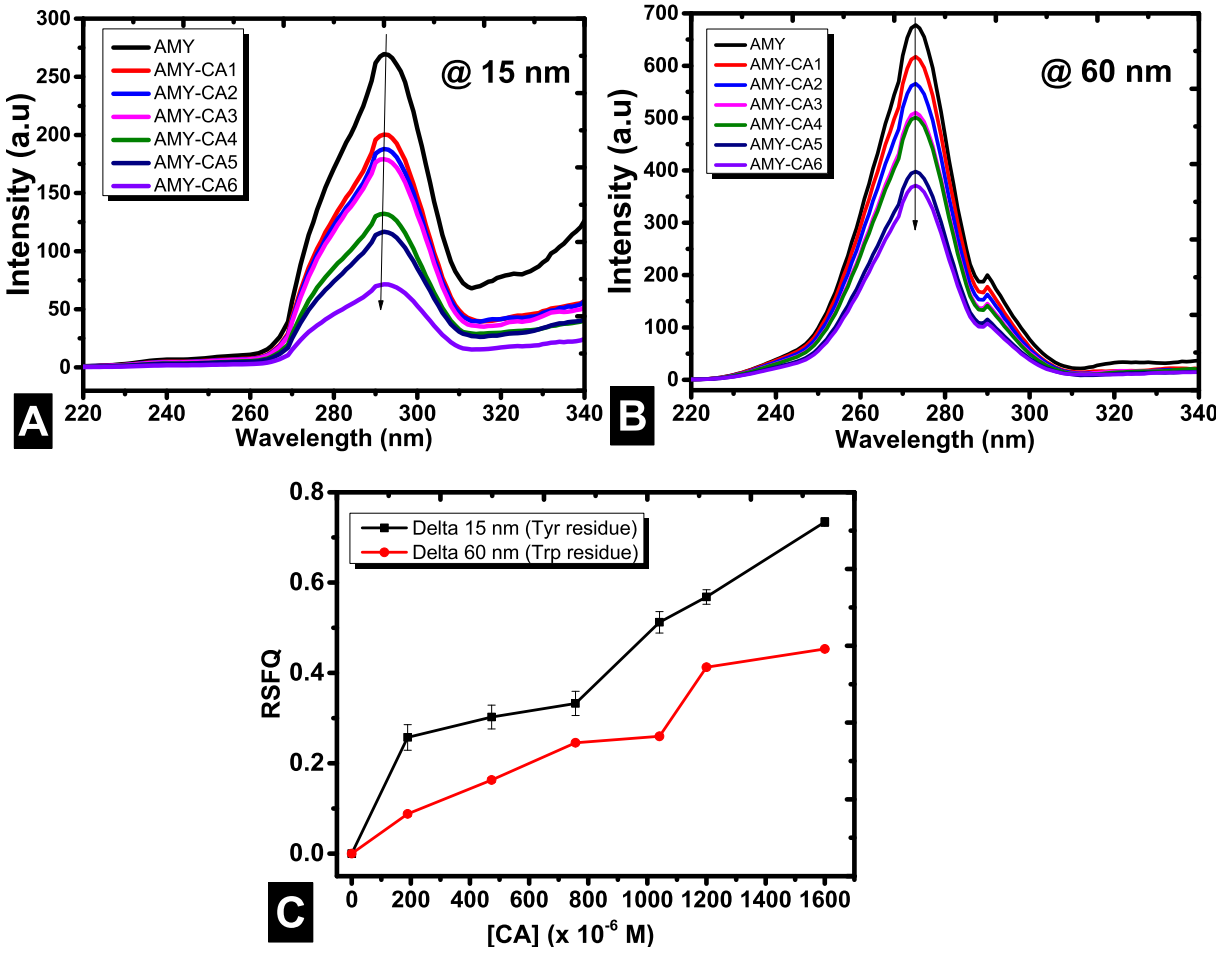


**Fig. 5.** Synchronous fluorescence spectra of α-amylase (AMY) at pH 7.4 in the presence of varying citric acid (CA) concentrations at Δλ 15 nm (A) and Δλ 60 nm (B). The plots of relative synchronous fluorescence quotients (C) showed AMY with higher quotient for Tyr than for Trp residues in the presence of CA.

of tryptophan residues in AMY in the presence of citric acid. This suggests that the binding of CA to AMY did not affect the microenvironment of Trp residues but that of Tyr residues in AMY. It could also be inferred that, unlike the Tyr residues, Trp residues in AMY were located at a significant distance from the citric acid and hence, avoided any effect or interaction [47]. To further affirm the impact of the binding interaction of citric acid on the microenvironments of tyrosine and tryptophan residues within the protein, plots of the relative synchronous fluorescence quotients of AMY in the presence of citric acid at Δλ = 15 nm and Δλ = 60 nm were made as shown in Fig. 5C. Usually, the microenvironment of tyrosine residues around a protein's binding site is said to be more affected than that of tryptophan residues when the value of slope at Δλ = 15 nm is higher than that at Δλ = 60 nm, and vice versa [2]. Our results showed that AMY had a higher quotient for Tyr residues [Slope = (4.07 ± 0.46) × $10^{-4}$ $M^{-1}$] than for Trp residues [Slope = (2.81 ± 0.27) × $10^{-4}$ $M^{-1}$] in the presence of citric acid. This affirmed that the microenvironment of tyrosine residues was significantly affected (unlike tryptophan residues) in AMY [2,47]. Our findings are in agreement with the report of [18] on the binding interaction of tannic acid with α-glucosidase.

### 3.2.4. 3-Dimensional fluorescence spectroscopy

3D fluorescence is a unique spectroscopic technique used in recent years for monitoring of changes in protein structures (secondary and tertiary structures) induced by ligand binding [17,42,48,49]. As revealed in the 3D fluorescence surface and contour plots (Fig. 6) for the interaction between AMY and CA, the AMY spectrum showed two Rayleigh scattering peaks [the first order Rayleigh scattering peak, called Peak 'a' (where $\lambda_{ex} = \lambda_{em}$) and the second order Rayleigh scattering, Peak 'b' (where $2\lambda_{ex} = \lambda_{em}$)] [50,51] and two major peaks (Peak 1 and Peak 2) [51-53]; both in the absence and presence of CA. The intensity of peak 'a' increased with the addition of citric acid (Fig. 6). This can be

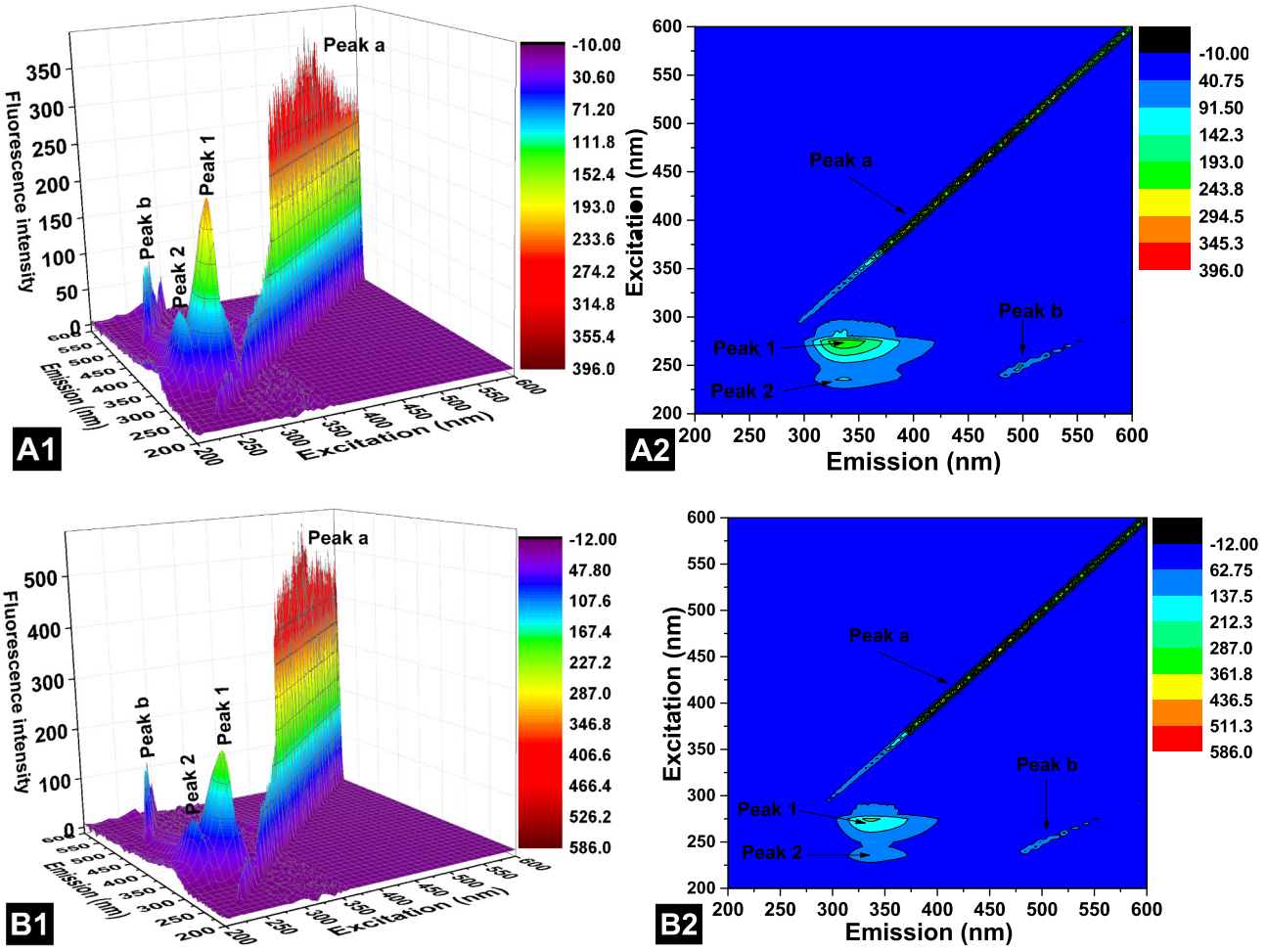


**Fig. 6.** 3D fluorescence spectra of AMY (8.93x10-6 M) in the absence and presence of citric acid at physiological pH 7.4 and 298 K. (A) AMY only; (B) AMY:CA (1:53).

ascribed to complex formation, and thus, a bigger macromolecule size resulted in higher scattering effect [50,51,53]. The peak 1 ($\lambda_{ex}/\lambda_{em}$: 275/336 nm; Intensity = 228.83 a.u.) in AMY (Fig. 6) is attributed to the intrinsic fluorescence spectral behaviour of tyrosine and tryptophan residues, whereas AMY peak 2 ($\lambda_{ex}/\lambda_{em}$: 235/336 nm; Intensity = 95.48 a.u.) (Fig. 6) is due to the excitation of higher excited electronic states of the enzyme's aromatic (Trp and Tyr) residues [51-53]. Hence both peaks (peak 1 and peak 2) account for the local environment of the aromatic residues (Trp and Tyr) but more importantly the peak 1. Previous claims in literature that wrongly adduced peak 2 to peptide backbone have been disproved [50]. From the respective 3D and contour plots of fluorescence analyses in Fig. 6A and Fig. 6B, the fluorescence intensity of peak 1 in the native enzyme AMY (Fig. 6A) decreased upon addition of citric acid in the AMY-CA system (Fig. 6B). Peak 2 was also mildly altered. The ratio of intensities ($F/F_o$) of peak 1 was 1: 0.97 for AMY: AMY-CA system. The observed peaks are mainly due to the fluorescent properties of aromatic residues (Tyr and Trp) in AMY (usually the impact of phenylalanine is very negligible and as such is not accounted for) and the alterations in the fluorescence intensities upon interaction with citric acid indicate some level of changes in the microenvironments in the AMY.

### 3.3. Thermodynamic parameters

Values of the thermodynamic parameters of a given reaction, including ligand–protein interactions, are generally used in predicting the spontaneity of the process as well as in delineating the driving forces in the reaction process [42,54]. The interaction between macromolecules (proteins) and small molecules (ligands) usually involve four major kinds of interaction forces, namely: electrostatic force, hydrophobic interaction, van der Waals force and hydrogen bond interaction [42,54]. In the present study, we estimated the enthalpy change ($\Delta H$) and entropy change ($\Delta S$) of the α-amylase – citric acid binding interaction using Van't Hoff equation (Eq. (12)) and a graph of natural logarithm of the binding association constant (In $K_a$) against reciprocal of temperature (in Kelvin) was plotted (Fig. 7).

$$InK_a = \frac{-\Delta H}{R}\left(\frac{1}{T}\right) + \frac{\Delta S}{R} \tag{12}$$

$$\Delta G = \Delta H - T\Delta S \tag{13}$$

where R denotes the universal gas constant (8.314 J/K/mol) and T is temperature in Kelvin.

Change in Gibb's free energy ($\Delta G$) was calculated based on Gibbs-Helmoholtz equation (Eq. (13)) and the corresponding thermodynamic parameters of the interaction between α-amylase and citric acid at physiological pH (pH 7.4) were summarized as shown in Table 3. Values of $\Delta G$ were negative at all the temperatures investigated. This showed that the binding interaction between α-amylase and citric acid occurred spontaneously [1,42]. According to Ross and Subramanian [55], the binding interaction between a protein and ligand is said to be governed by electrostatic forces if

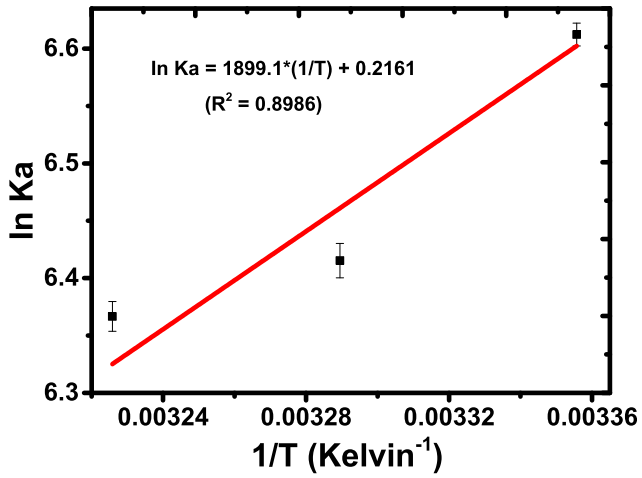


**Fig 7.** Van't Hoff's plot for the binding interaction of α-amylase and citric acid at pH 7.4.

the change in enthalpy is negative (ΔH < 0) and entropy change is positive (ΔS > 0). In the present study, ΔH = -15.79 kJmol$^{-1}$ and ΔS = 0.002 kJmol$^{-1}$ as shown in Table 3. Hence, this suggests that the binding interaction between citric acid and alpha-amylase was driven mostly by electrostatic forces. The likely involvement of electrostatic forces in the CA-AMY binding interaction could be attributed to the fact that citric acid, being a tricarboxylic acid, could easily dissociate at physiological pH and thereafter interact with positively charged amino acid residues in the enzyme [54,56]. Further, TΔS was greater than ΔH suggesting that the reaction was driven by entropy (Table 3). It should, however, be noted that since the reaction took place in an aqueous medium the possibility of also having some hydrogen bond interactions may not be alien as indicated by the molecular docking results (Section 3.8).

### 3.4. Anti-glycation properties of CA

Advanced glycation end-products (AGEs) are generally heterogenous in nature, among which many are known to emit fluorescence when excited at a specific wavelength [20,46]. AGEs have been widely reported to aggravate complications in patients with diabetes mellitus, cardiovascular diseases as well as in age-related diseases. Hence in the present study, the protective effect of citric acid against formation of advanced glycation end-products was investigated using fluorescence spectroscopy. Non-enzymatic protein glycation was induced by fructose in the absence of CA and aminoguanidine, while other experimental set-ups contained the glycated protein (bovine serum albumin, BSA) in the presence of varying concentrations of CA and aminoguanidine (AG, a standard anti-glycation agent) (Fig. 8). Fig. 8A shows the emission fluorescence spectra of native BSA, glycated BSA, and glycated BSA treated respectively with citric acid (Fig. 8A1) and aminoguanidine (Fig. 8A2). The fluorescence intensity of the glycated BSA was very strong (28.58% higher than that of control BSA), indicating the presence of AGEs in the glycated BSA [46]. When compared to the glycated BSA (BSA-Fru group), increasing concentrations of citric acid and aminoguanidine resulted in steady decrease in the fluorescence intensity of the glycated BSA (Fig. 8A1 and Fig. 8A2). This revealed that these compounds (CA and AG) inhibited formation of AGEs. From the regression plots of relative anti-glycation (%) against concentration of CA or AG shown in Fig. 8B1 and Fig. 8B2, the protective effects of CA and AG against fructose-induced protein glycation were concentration-dependent. The half-minimal inhibitory concentrations ($IC_{50}$) of citric acid and aminoguanidine against AGEs formation were calculated to be 0.795 ± 0.001 and 0.853 ± 0.005 mM, respectively. This suggested that CA exhibited a strong anti-glycation potential, slightly higher than that of the standard anti-glycation agent (AG). Our anti-glycation result is in agreement with previous reports in which galangin and naringenin were investigated instead of citric acid [20,46].

### 3.5. Inhibitory effect of CA on α-amylase and inhibition kinetics

The effect of citric acid on α-amylase activity was investigated in the present study by using a standard biochemical assay protocol [11,21] and the regression plot of percentage α-amylase inhibition against citric acid concentration was drawn as shown in Fig. 9a. The result showed that CA inhibited α-amylase hydrolytic activity in a concentration-dependent manner (Fig. 9a). Fifty percent (50%) of α-amylase activity was inhibited by citric acid at a concentration ($IC_{50}$) of 5.01 ± 0.87 mM (Fig. 9a). The $IC_{50}$ value of CA for α-amylase was low, which affirmed its high capacity to suppress AMY activity. The $IC_{50}$ value of acarbose [$IC_{50}$ = 168.69 μM (i.e 108.91 μg/mL)] obtained for the same enzyme under similar experimental conditions was, however, lower than that of CA for α-amylase [7]. This indicated that the inhibitory effect of acarbose on AMY activity is higher than that of CA [3,6]. It should, however, be noted that the relatively reduced AMY inhibitory effect of CA (compared to the standard drug, acarbose) is highly desirable since intake of CA would not only result in gradual suppression of starch hydrolysis by α-amylase but would also help to prevent challenges associated with intake of acarbose whose excessively high inhibitory action on starch hydrolysis culminates in eventual abdominal discomfort, flatulence and diarrhea [7].

The mode of inhibition and inhibition kinetic parameters were determined with the aid of primary and secondary Lineweaver-Burk (LB) plots. In the primary LB plot in Fig. 9b, the lines of inhibition plots in the presence of different concentrations of the inhibitor (CA) neither intercepted at the vertical axis nor at the horizontal axis but slightly within the second quadrat of the graph. This indicated that CA inhibited AMY by a mixed mode of inhibition [22]. The secondary LB plots (Fig. 9b inserts, SLB 1 and SLB 2) were used to deduce the values of the inhibition constants for competitive inhibition ($K_{ic}$) and uncompetitive inhibition ($K_{iu}$) potentials, respectively. $K_{ic}$ denotes the affinity of the inhibitor for the free enzyme, while $K_{iu}$ represents the inhibitor's affinity towards binding of the enzyme-substrate complex. Similar to the fact that decreased values of $IC_{50}$ implied increased inhibition

**Table 3**
Thermodynamics properties of the binding interaction of α-amylase and citric acid at pH 7.4.

| Temperature (K) | ΔH (kJ/mol) | ΔG (kJ/mol) | ΔS (kJ/mol) | TΔS (kJ.K./mol) |
|---|---|---|---|---|
| 298 | −15.79 | −16.32 | 0.002 | 0.535 |
| 303 | | −16.33 | | 0.544 |
| 310 | | −16.35 | | 0.557 |

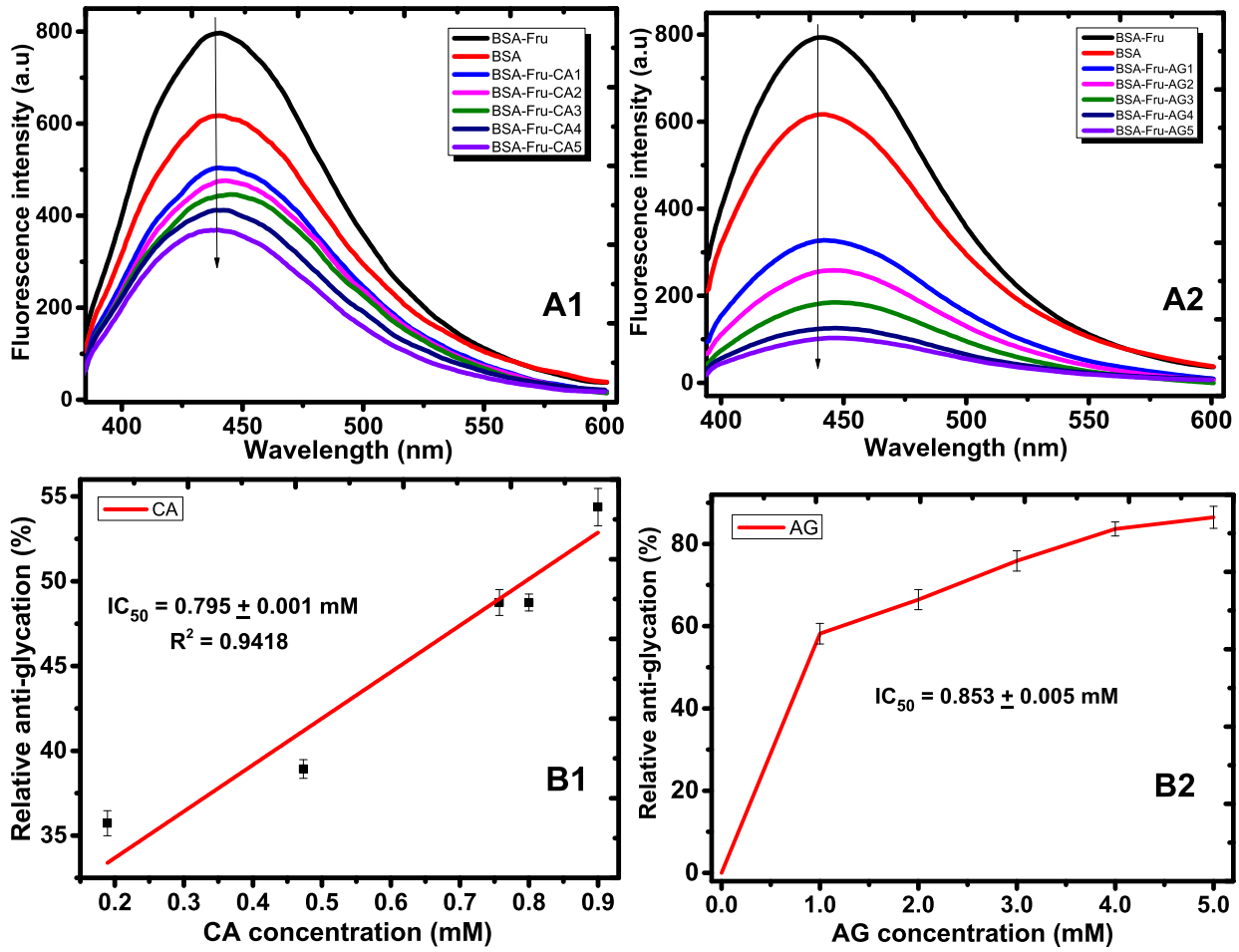


**Fig. 8.** Protective effects of citric acid (CA) and aminoguanidine (AG) against fructose-induced bovine serum albumin (BSA) glycation *in vitro*. A1 and A2 denote fluorescence intensity of glycated BSA in the absence and presence of citric acid and aminoguanidine, respectively; (B) Relative anti-glycation (%) of citric acid (B1) and the standard protein glycation inhibitor, aminoguanidine hydrochloride (B2).

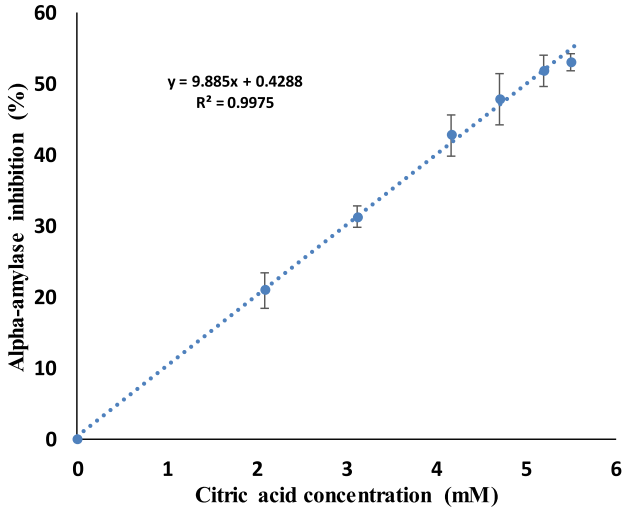


**Fig. 9a.** Inhibitory effect of citric acid on alpha-amylase activity.

strength of the inhibitor, values of $K_{ic}$ or $K_{iu}$ are lower when the inhibition type described by the parameter is stronger or more prevalent [57]. The reverse is, however, the case with the reciprocals of $K_{ic}$ or $K_{iu}$. The results shown in Table 4 showed that $K_{ic} < K_{iu}$ value (or $1/K_{ic} > 1/K_{iu}$ value), suggesting that the mixed inhibitor (citric acid) inhibited α-amylase predominantly via competitive mode of inhibition and sparingly via uncompetitive inhibition mode [22,57].

### 3.6. Molecular docking analysis

The computational analysis of the binding interaction between AMY and CA indicated that α-amylase interacted with citric acid at the enzyme's active site with a binding affinity of −5.4 kcal/mol. However, it interacted with acarbose with a binding affinity of −7.9 kcal/mol (Table 5). Computational evidence of binding of drug leads to the active site of α-amylase has shown that in addition to the catalytic triad of amino acids identified by x-ray crystallography, other neighboring amino acids may also be involved in ligand binding [58]. CA interaction with AMY occurred through amino acid residues such as His-101, Asp-197, Glu-233 and His-299 at the active site of α-amylase (Fig. 10; Table 5), while acarbose (a standard α-amylase inhibitor and hypoglycemic agent) was however predicted to interact with Gln-63, Trp-59, Val-163, Asp-197, Asp-300 and Glu-233 at the active site of α-amylase. It has been widely reported that Asp-197, Glu-233 and Asp-300 comprised the catalytic triad of alpha-amylases [58]. From the results obtained, citric acid inter-

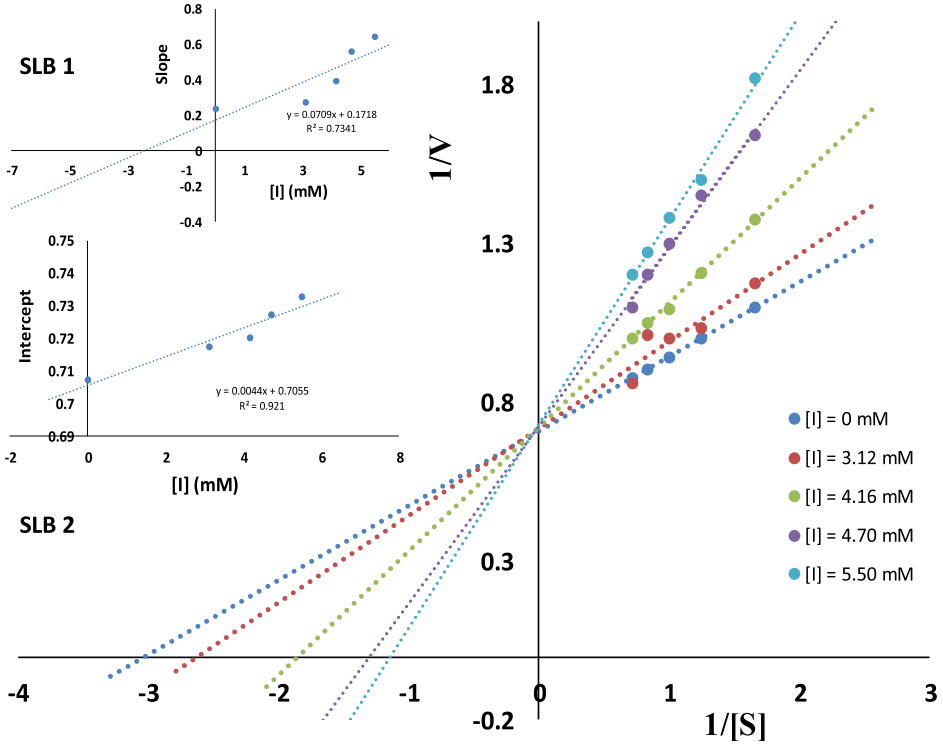


**Fig. 9b.** Lineweaver-Burk (LB) plot for α-amylase activity at pH 7.4 in the absence and presence of citric acid. Inserts: SLB1 and SLB2 are secondary LB plots for estimation of inhibition constants ($K_{ic}$ and $K_{iu}$, respectively).

**Table 4**
Detailed kinetic parameters of α-amylase in the presence of citric acid.

| Parameter | Value |
|---|---|
| $K_{ic}$ (mM) | 2.42 |
| $K_{iu}$ (mM) | 160.34 |
| $1/K_{ic}$ ($mM^{-1}$) | 0.413 |
| $1/K_{iu}$ ($mM^{-1}$) | 0.006 |
| Inhibitor type | Mixed |
| $IC_{50}$ (mM) | 5.01 ± 0.87 |

**Table 5**
Molecular interactions of ligands with α-amylase.

| Ligand | Binding affinity (kcal/mol) | Interacting residues |
|---|---|---|
| Citric acid | −5.4 | H-bonds: His-101 (2.26 Å), Asp-197 (2.36 Å), Glu-233 (2.41 Å), His-299 (2.01 Å) |
| Acarbose | −7.9 | H-bonds: Trp-59 (2.35 Å), Gln-63 (1.97 Å), Val-163 (2.21 Å), Asp-197 (2.39 Å), Glu-233 (2.41 Å), Asp-300 (2.43 Å) |

acted with some of the amino acid residues (Asp-197, Glu-233) known to be involved in catalysis and stabilization of the AMY active site domain almost as acarbose did (Asp-197, Asp-300 and Glu-233) (Fig. 10). This, in addition to α-amylase's moderately high binding affinity for CA, could probably account for the observed inhibitory prowess of citric acid on α-amylase activity reported in the present study.

## 4. Conclusions

In this study, the binding interaction of a starch-hydrolyzing enzyme (α-amylase) with a common food preservative (citric acid) was studied using multiple spectroscopic methods; followed by investigation of the anti-glycation potential of citric acid. The intrinsic fluorescence intensity of tryptophan and tyrosine residues in α-amylase was quenched by CA via a static mechanism, indicating complex formation between AMY and CA. UV–visible absorption spectroscopy, FT-IR and 3D fluorescence spectroscopy all affirmed alteration in the native conformation of AMY due to its

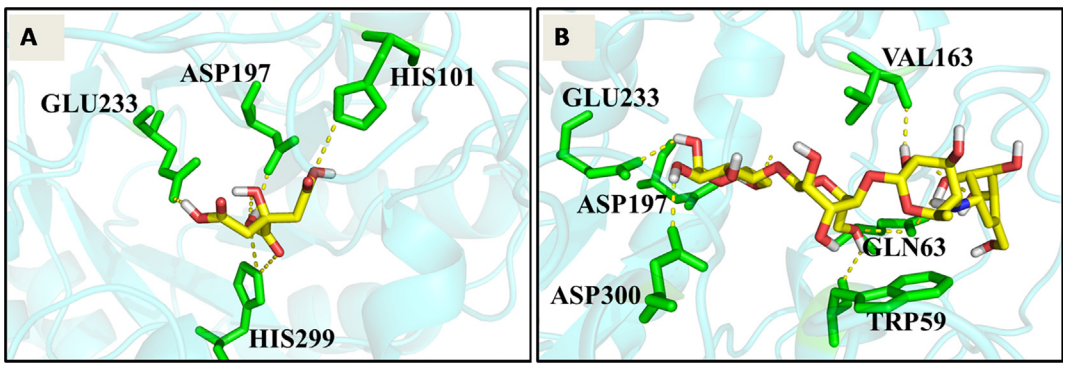


**Fig. 10.** Lowest binding energy poses of citric acid (A) and acarbose (B) to α-amylase.

interaction with CA. Values of the binding constant ($K_a$) obtained from experimental results and binding affinity obtained from molecular docking analysis showed good agreement that CA was moderately bound to AMY and that led to its observed inhibitory action on AMY activity. CA suppressed α-amylase activity via a mixed mode of inhibition with values of inhibition constants in the order, $K_{ic} < K_{iu}$. CA also strongly inhibited fructose-induced formation of advanced glycation end-products (AGEs) with an $IC_{50}$ of 0.795 ± 0.001 mM, slightly higher than that of aminoguanidine (a standard anti-glycation agent). Our findings showed that CA could impair formation of AGEs and interact with α-amylase to slow down its starch-hydrolyzing activity, vital properties of agents with potential for management of complications in type 2 diabetes.

*CRediT authorship contribution statement*

**Oghenetega J. Avwioroko:** Conceptualization, Methodology, Supervision, Validation, Writing – original draft, Writing – review & editing, Writing – original draft. **Akpovwehwee A. Anigboro:** Conceptualization, Methodology, Supervision, Validation, Writing – original draft, Writing – review & editing. **Chiagoziem A. Otuechere:** Conceptualization, Methodology, Supervision, Validation, Writing – original draft, Writing – review & editing. **Francis O. Atanu:** Conceptualization, Methodology, Supervision, Validation, Writing – original draft, Writing – review & editing. **Oluropo F. Dairo:** Conceptualization, Methodology, Supervision, Validation, Writing – original draft, Writing – review & editing. **Temidayo T. Oyetunde:** Conceptualization, Methodology, Writing – original draft, Writing - review & editing. **Omotayo B. Ilesanmi:** Conceptualization, Methodology, Supervision, Validation, Writing – original draft, Writing – review & editing. **Augustine Apiamu:** Conceptualization, Methodology, Writing – original draft, Writing - review & editing. **Akpoyovware S. Ejoh:** Conceptualization, Methodology, Writing – original draft, Writing – review & editing. **Damilare Olorunnisola:** Methodology, Writing – original draft, Writing - review & editing. **Moses O. Alfred:** Methodology, Writing – original draft, Writing - review & editing. **Martins O. Omorogie:** Conceptualization, Methodology, Supervision, Validation, Writing – original draft, Writing – review & editing. **Nyerhovwo J. Tonukari:** Conceptualization, Methodology, Supervision, Validation, Writing – original draft, Writing – review & editing.

## Declaration of Competing Interest

The authors declare that they have no known competing financial interests or personal relationships that could have appeared to influence the work reported in this paper.

## Acknowledgements

The authors sincerely appreciate the efforts of all laboratory assistants and technical personnel who contributed to the overall success of this research work.

Funding.

This research did not receive any specific grant from funding agencies in the public, commercial, or not-for-profit sector.

## References

[1] O.J. Avwioroko, T.T. Oyetunde, F.O. Atanu, C.A. Otuechere, A.A. Anigboro, O.F. Dairo, A.S. Ejoh, S.O. Ajibade, M.O. Omorogie, Exploring the binding interactions of structurally diverse dichalcogenoimidodiphosphinate ligands with α-amylase: Spectroscopic approach coupled with molecular docking, Biochem. Biophys. Rep. 24 (2020) 100837.

[2] O.J. Avwioroko, A.A. Anigboro, F.O. Atanu, C.A. Otuechere, M.O. Alfred, J.N. Abugo, M.O. Omorogie, Investigation of the binding interaction of α-amylase with Chrysophyllum albidum seed extract and its silver nanoparticles: A multi-spectroscopic approach, Chem. Data Collect. 29 (2020) 100517.

[3] H. Yaribeygi, T. Sathyapalan, S.L. Atkin, A. Sahebkar, Molecular mechanisms linking oxidative stress and diabetes mellitus, Oxidative Medicine Cellular Longevity 2020 (2020) 1–13.

[4] U. Magaji, O. Sacan, R. Yanardag, Alpha amylase, alpha glucosidase and glycation inhibitory activity of Moringa oleifera extracts, S. Afr. J. Bot. 128 (2020) 225–230.

[5] A. Ahmad, A. Zafar, S. Zargar, A. Bazgaifan, T.A. Wani, M. Ahmad, Protective effects of apigenin against edifenphos-induced genotoxicity and cytotoxicity in rat hepatocytes, Journal of Biomolecular Structure Dynamics (2021) 1–16.

[6] S.A. Adefegha, G. Oboh, Inhibition of key enzymes linked to type 2 diabetes and sodium nitroprusside-induced lipid peroxidation in rat pancreas by water extractable phytochemicals from some tropical spices, Pharm. Biol. 50 (7) (2012) 857–865.

[7] A.A. Anigboro, O.J. Avwioroko, O.A. Ohwokevwo, B. Pessu, N.J. Tonukari, Phytochemical profile, antioxidant, α-amylase inhibition, binding interaction and docking studies of Justicia carnea bioactive compounds with α-amylase, Biophys. Chem. 269 (2021) 106529.

[8] O.J. Avwioroko, A.A. Anigboro, A.S. Ejoh, F.O. Atanu, M.A. Okeke, N.J. Tonukari, Characterization of α-amylases isolated from Cyperus esculentus seeds (tigernut): biochemical features, kinetics and thermal inactivation thermodynamics, Biocatalysis and Agricultural Biotechnology 21 (2019) 101298.

[9] F.O. Atanu, O.J. Avwioroko, S. Momoh, Anti-diabetic effect of combined treatment with Aloe vera gel and Metformin on alloxan-induced diabetic rats, Journal of Ayurvedic Herbal Medicine 4 (1) (2018) 1–5.

[10] A. Atanu FO, A. Avwioroko OJ, I. Ilesanmi OB, O.M. Oguche M, Comparative study of the effects of Annona muricata and Tapinanthus globiferus extracts on biochemical indices of diabetic rats, Pharmacognosy Journal 11 (6) (2019) 1365–1370.

[11] G. Oboh, O.B. Ogunsuyi, M.D. Ogunbadejo, S.A. Adefegha, Influence of gallic acid on α-amylase and α-glucosidase inhibitory properties of acarbose, Journal of Food Drug, Analysis 24 (2016) 627–634.

[12] S. Priya, N. Kaur, A.K. Gupta, Purification, characterization and inhibition studies of α-amylase of Rhyzopertha dominica, Pesticide Biochemistry, Physiology 98 (2010) 231–237.

[13] J.-H. Shi, D.-Q. Pan, M. Jiang, T.-T. Liu, Q. Wang, Binding interaction of ramipril with bovine serum albumin (BSA): Insights from multi-spectroscopy and molecular docking methods, Journal of Photochemistry Photobiology B: Biology 164 (2016) 103–111.

[14] M. Makarska-Bialokoz, A. Lipke, Study of the binding interactions between uric acid and bovine serum albumin using multiple spectroscopic techniques, J. Mol. Liq. 276 (2019) 595–604.

[15] T.A. Wani, A.H. Bakheit, A.A. Al-Majed, N. Altwaijry, A. Baquaysh, A. Aljuraisy, S. Zargar, Binding and drug displacement study of colchicine and bovine serum albumin in presence of azithromycin using multispectroscopic techniques and molecular dynamic simulation, J. Mol. Liq. 333 (2021) 115934.

[16] T.A. Wani, N.A. Alsaif, M.M. Alanazi, A.H. Bakheit, A.A. Khan, S. Zargar, Binding of colchicine and ascorbic acid (vitamin C) to bovine serum albumin: An in-vitro interaction study using multispectroscopic, molecular docking and molecular dynamics simulation study, J. Mol. Liq. 342 (2021) 117542.

[17] B.-L. Wang, D.-Q. Pan, S.-B. Kou, Z.-Y. Lin, J.-H. Shi, Exploring the binding interaction between bovine serum albumin and perindopril as well as influence of metal ions using multi-spectroscopic, molecular docking and DFT calculation, Chem. Phys. 530 (2020) 110641.

[18] Q. Huang, W.-M. Chai, Z.-Y. Ma, C. Ou-Yang, Q.-M. Wei, S. Song, Z.-R. Zou, Y.-Y.J. I.j.o.b.m. Peng, Inhibition of α-glucosidase activity and non-enzymatic glycation by tannic acid: Inhibitory activity and molecular mechanism, 141 (2019) 358-368.

[19] N.A. Alsaif, T.A. Wani, A.H. Bakheit, S. Zargar, Multi-spectroscopic investigation, molecular docking and molecular dynamic simulation of competitive interactions between flavonoids (quercetin and rutin) and sorafenib for binding to human serum albumin, Int. J. Biol. Macromol. 165 (2020) 2451–2461.

[20] L. Zeng, H. Ding, X. Hu, G. Zhang, D. Gong, Galangin inhibits α-glucosidase activity and formation of non-enzymatic glycation products, Food Chem. 271 (2019) 70–79.

[21] X.-J. Li, Z.-G. Li, X. Wang, J.-Y. Han, B. Zhang, Y.-J. Fu, C.-J. Zhao, Application of cavitation system to accelerate aqueous enzymatic extraction of seed oil from Cucurbita pepo L. and evaluation of hypoglycemic effect, Food Chem. 212 (2016) 403–410.

[22] A.A. Anigboro, O.J. Avwioroko, O. Akeghware, N.J. Tonukari, Anti-obesity, antioxidant and in silico evaluation of Justicia carnea bioactive compounds as potential inhibitors of an enzyme linked with obesity: Insights from kinetics, semi-empirical quantum mechanics and molecular docking analysis, Biophys. Chem. 274 (2021) 106607.

[23] N. Cardullo, V. Muccilli, L. Pulvirenti, A. Cornu, L. Pouységu, D. Deffieux, S. Quideau, C. Tringali, C-glucosidic ellagitannins and galloylated glucoses as potential functional food ingredients with anti-diabetic properties: A study of α-glucosidase and α-amylase inhibition, Food Chem. 313 (2020) 126099.

[24] B.A. Falese, A.N. Kolawole, O.A. Sarumi, A.O. Kolawole, Probing the interaction of iminium form of sanguinarine with human salivary α-amylase by multi-spectroscopic techniques and molecular docking, J. Mol. Liq. 334 (2021) 116346.

[25] X. Yu, X. Cai, S. Li, L. Luo, J. Wang, M. Wang, L. Zeng, Studies on the interactions of theaflavin-3, 3′-digallate with bovine serum albumin: Multi-spectroscopic analysis and molecular docking, Food Chem. 366 (2022) 130422.

[26] A.A. Al-Mehizia, A.H. Bakheit, S. Zargar, M.A. Bhat, M.M. Asmari, T.A. Wani, Evaluation of biophysical interaction between newly synthesized pyrazoline pyridazine derivative and bovine serum albumin by spectroscopic and molecular docking studies, Journal of Spectroscopy 2019 (2019) 1–12.
[27] S. Zargar, S. Alamery, A.H. Bakheit, T.A. Wani, Poziotinib and bovine serum albumin binding characterization and influence of quercetin, rutin, naringenin and sinapic acid on their binding interaction, Spectrochimica Acta Part A: Molecular Biomolecular Spectroscopy 235 (2020) 118335.
[28] T.A. Wani, A.H. Bakheit, S. Zargar, M.A. Bhat, A.A. Al-Majed, Molecular docking and experimental investigation of new indole derivative cyclooxygenase inhibitor to probe its binding mechanism with bovine serum albumin, Bioorg. Chem. 89 (2019) 103010.
[29] P.K. Borah, A. Sarkar, R.K.J.F.c. Duary, Water-soluble vitamins for controlling starch digestion: Conformational scrambling and inhibition mechanism of human pancreatic α-amylase by ascorbic acid and folic acid, 288 (2019) 395-404.
[30] H.F. Crouse, E.M. Petrunak, A.M. Donovan, A.C. Merkle, B.L. Swartz, S. Basu, Static and dynamic quenching of tryptophan fluorescence in various proteins by a chromium (III) complex, Spectrosc. Lett. 44 (2011) 369–374.
[31] N.A. Alsaif, A.A. Al-Mehizia, A.H. Bakheit, S. Zargar, T.A. Wani, A spectroscopic, thermodynamic and molecular docking study of the binding mechanism of dapoxetine with calf thymus DNA, South African, J. Chem. 73 (2020) 44–50.
[32] Y.-F. Zhang, K.-L. Zhou, Y.-Y. Lou, D.-q. Pan, J.-H. Shi, Investigation of the binding interaction between estazolam and bovine serum albumin: multi-spectroscopic methods and molecular docking technique, Journal of Biomolecular Structure, Dynamics 35 (16) (2017) 3605–3614.
[33] Q. Wang, C.-R. Huang, M. Jiang, Y.-Y. Zhu, J. Wang, J. Chen, J.-H. Shi, Binding interaction of atorvastatin with bovine serum albumin: Spectroscopic methods and molecular docking, Spectrochimica Acta Part A: Molecular Biomolecular, Spectroscopy 156 (2016) 155–163.
[34] J.R. Lakowicz, Protein fluorescence, in: J.R. Lakowicz (Ed.), Principles of Fluorescence Spectroscopy, Springer US, Boston, MA, 1983, pp. 341–381.
[35] B.-L. Wang, D.-Q. Pan, K.-L. Zhou, Y.-Y. Lou, J.-H. Shi, Multi-spectroscopic approaches and molecular simulation research of the intermolecular interaction between the angiotensin-converting enzyme inhibitor, ACE inhibitor) benazepril and bovine serum albumin (BSA, Spectrochimica Acta Part A: Molecular Biomolecular Spectroscopy 212 (2019) 15–24.
[36] M. Wang, J. Shi, L. Wang, Y. Hu, X. Ye, D. Liu, J. Chen, Inhibitory kinetics and mechanism of flavonoids from lotus (Nelumbo nucifera Gaertn.) leaf against pancreatic α-amylase, Int. J. Biol. Macromol. 120 (2018) 2589–2596.
[37] R. Gan, L. Zhao, Q. Sun, P. Tang, S. Zhang, H. Yang, J. He, H. Li, Binding behavior of trelagliptin and human serum albumin: Molecular docking, dynamical simulation, and multi-spectroscopy, Spectrochimica Acta Part A: Molecular Biomolecular, Spectroscopy 202 (2018) 187–195.
[38] Q. Lu, C. Chen, S. Zhao, F. Ge, D. Liu, Investigation of the interaction between gallic Acid and α-amylase by spectroscopy, Int. J. Food Prop. 19 (2016) 2481–2494.
[39] S. Bi, L. Ding, Y. Tian, D. Song, X. Zhou, X. Liu, H. Zhang, Investigation of the interaction between flavonoids and human serum albumin, J. Mol. Struct. 703 (2004) 37–45.
[40] S.R. Feroz, S.B. Mohamad, Z.S. Bakri, S.N. Malek, S. Tayyab, Probing the interaction of a therapeutic flavonoid, pinostrobin with human serum albumin: multiple spectroscopic and molecular modeling investigations, PLoS ONE 8 (2013) e76067.
[41] M. Van de Weert, L. Stella, Fluorescence quenching and ligand binding: A critical discussion of a popular methodology, J. Mol. Struct. 998 (2011) 144–150.
[42] S.-B. Kou, Z.-Y. Lin, B.-L. Wang, J.-H. Shi, Y.-X. Liu, Evaluation of the interaction of novel tyrosine kinase inhibitor apatinib mesylate with bovine serum albumin using spectroscopies and theoretical calculation approaches, Journal of Biomolecular Structure Dynamics 39 (13) (2021) 4795–4806.
[43] S. Tayyab, L.H. Min, M.Z. Kabir, S. Kandandapani, N.F.W. Ridzwan, S.B. Mohamad, Exploring the interaction mechanism of a dicarboxamide fungicide, iprodione with bovine serum albumin, Chem. Pap. 74 (2020) 1633–1646.
[44] A.B.M. Giasuddin, D.W. Britt, Microwave assisted sol-gel synthesis of silica-spider silk composites, Molecules 24 (2019) 2521.
[45] R.-J. Zhang, S.-B. Kou, L. Hu, L. Li, J.-H. Shi, S.-L. Jiang, Exploring binding interaction of baricitinib with bovine serum albumin (BSA): multi-spectroscopic approaches combined with theoretical calculation, J. Mol. Liq. 354 (2022) 118831.
[46] M.S. Khan, F.A. Qais, M.T. Rehman, M.H. Ismail, M.S. Alokail, N. Altwaijry, N.O. Alafaleq, M.F. AlAjmi, N. Salem, R. Alqhatani, Mechanistic inhibition of non-enzymatic glycation and aldose reductase activity by naringenin: Binding, enzyme kinetics and molecular docking analysis, Int. J. Biol. Macromol. 159 (2020) 87–97.
[47] M. Konar, H. Sahoo, Tyrosine mediated conformational change in bone morphogenetic protein–2: Biophysical implications of protein–phytoestrogen interaction, Int. J. Biol. Macromol. 150 (2020) 727–736.
[48] S. Rahman, M.T. Rehman, G. Rabbani, P. Khan, M.F. AlAjmi, M. Hassan, G. Muteeb, J. Kim, Insight of the interaction between 2, 4-thiazolidinedione and human serum albumin: a spectroscopic, thermodynamic and molecular docking study, Int. J. Mol. Sci. 20 (2019) 2727.
[49] B. Sandhya, A.H. Hegde, S.S. Kalanur, U. Katrahalli, J. Seetharamappa, Interaction of triprolidine hydrochloride with serum albumins: thermodynamic and binding characteristics, and influence of site probes, Journal of Pharmaceutical Biomedical, Analysis 54 (2011) 1180–1186.
[50] A. Bortolotti, Y.H. Wong, S.S. Korsholm, N.H.B. Bahring, S. Bobone, S. Tayyab, M. van de Weert, L. Stella, On the purported "backbone fluorescence" in protein three-dimensional fluorescence spectra, RSC Adv. 6 (114) (2016) 112870–112876.
[51] S. Siddiqui, F. Ameen, T. Kausar, S.M. Nayeem, S. Ur Rehman, M. Tabish, Biophysical insight into the binding mechanism of doxofylline to bovine serum albumin: An in vitro and in silico approach, Spectrochimica Acta Part A: Molecular Biomolecular Spectroscopy 249 (2021) 119296.
[52] S. Das, P. Khanikar, Z. Hazarika, M.A. Rohman, A. Uzir, A. Nath Jha, A. Singha Roy, Deciphering the interaction of 5, 7-dihydroxyflavone with hen-egg-white lysozyme through multispectroscopic and molecular dynamics simulation approaches, ChemistrySelect 3 (17) (2018) 4911–4922.
[53] S. Das, N. Bora, M.A. Rohman, R. Sharma, A.N. Jha, A. Singha Roy, Molecular recognition of bio-active flavonoids quercetin and rutin by bovine hemoglobin: an overview of the binding mechanism, thermodynamics and structural aspects through multi-spectroscopic and molecular dynamics simulation studies, PCCP 20 (33) (2018) 21668.
[54] H. Tang, F. Ma, D. Zhao, Z. Xue, Exploring the effect of salvianolic acid C on α-glucosidase: Inhibition kinetics, interaction mechanism and molecular modelling methods, Process Biochem. 78 (2019) 178–188.
[55] P.D. Ross, S. Subramanian, Thermodynamics of protein association reactions: forces contributing to stability, Biochemistry 20 (1981) 3096–3102.
[56] J.C.N. Santos, I.M. da Silva, T.C. Braga, A. de Fatima, I.M. Figueiredo, J.C.C. Santos, Thimerosal changes protein conformation and increase the rate of fibrillation in physiological conditions: spectroscopic studies using bovine serum albumin, BSA, Int. J. Biol. Macromol. 113 (2018) 1032–1040.
[57] S. Wang, Y. Li, D. Huang, S. Chen, Y. Xia, S. Zhu, The inhibitory mechanism of chlorogenic acid and its acylated derivatives on α-amylase and α-glucosidase, Food Chem. 131334 (2021).
[58] C. Proença, M. Freitas, D. Ribeiro, S.M. Tomé, E.F. Oliveira, M.F. Viegas, A.N. Araújo, M.J. Ramos, A.M. Silva, P.A. Fernandes, Evaluation of a flavonoids library for inhibition of pancreatic α-amylase towards a structure–activity relationship, J. Enzyme Inhibition Med. Chem. 34 (2019) 577–588.